

Imidazo[4,5-*b*]pyridine derived iminocoumarins as potential pH probes: Synthesis, spectroscopic and computational studies of their protonation equilibria

Ida Boček,¹ Marijana Hranjec^{1*} and Robert Vianello^{2*}

¹Department of Organic Chemistry, Faculty of Chemical Engineering and Technology, University of Zagreb, Marulićev trg 19, 10000 Zagreb, Croatia.

²Laboratory for the Computational Design and Synthesis of Functional Materials, Division of Organic Chemistry and Biochemistry, Ruđer Bošković Institute, Bijenička 54, 10000 Zagreb, Croatia.

*Corresponding authors: mhranjec@fkit.hr (M.H.), robert.vianello@irb.hr (R.V.)

Abstract: We describe the synthesis, spectroscopic characterization and computational analysis of the protonation equilibria of several newly designed imidazo[4,5-*b*]pyridine derived iminocoumarins to confirm their potential as pH sensing molecules in different solvents. The photophysical characterization and acid/base properties of these chromophores have been carried out in several polar and non-polar organic solvents as well as buffered aqueous solution with different pH values using UV-Vis and fluorescence spectroscopies. Obtained results revealed that both the solvent polarity and the electronic nature of substituents placed at the iminocoumarin and imidazo[4,5-*b*]pyridine cores significantly influence spectral responses of studied systems. An excellent agreement in experimentally measured and computationally determined pK_a values and electronic excitations suggests that all systems are monoprotinated cations at neutral pH, while their transition to diprotinated forms occurs at pH values between 3.4 and 4.4, whereas they get reverted to neutral unionized molecules between 10.4 and 13.7. These small differences in narrow ranges of borderline pH values are predominantly brought about by variations in a single substituent on the iminocoumarin core, thereby allowing a simple strategy to further modify the observed sensing features and easily tune them for a specific application.

Keywords: imidazo[4,5-*b*]pyridines, iminocoumarins, pH sensitivity, prototropic equilibrium, computational chemistry, DFT and TD-DFT calculations

1. Introduction

Coumarin derivatives have established themselves among most important fluorescent organic compounds with a broad applicability in a wide range of photophysical applications [1–3]. Besides the fact that naturally occurring and synthetically prepared coumarins have diverse biological activities, they have attracted much attention as photonic materials and have been used as fluorescent brighteners [4,5], solar energy collectors [6,7], laser dyes [8] and organic nonlinear optical materials [9,10], owing this potential to their reasonable stability, good solubility and interesting photochemical characteristics [11]. Furthermore, they have also been used as charge-transfer agents [12,13], fluorescent labels [14], pigments and probes for physiological measurements in living systems [15,16], for the coloring of textile fibers and other materials [17], and corrosion inhibitors, [18] to mention only a few areas where they have been recognized as functional materials. Apart from their intrinsic electronic features, their spectral responses can be further modified upon substitution, leading to their appealing spectroscopic properties [19,20]. It is well demonstrated that the substitution at position 7 with electron-donating groups along with attaching the electron-accepting moieties at position 3, can considerably alter the fluorescence intensity of the prepared derivatives, mostly resulting in the red shifted absorption [21,22]. These photophysical properties can additionally be modulated by introducing a longer π -electronic conjugation, as it was revealed, for example, in several benzo- and benzazole-derived coumarins [23,24].

On the other hand, iminocoumarin derivatives are proven to be very promising materials with attractive optical properties, thereby allowing potential application as optical fluorescent materials [25]. Since there is a limited literature describing their optical characteristics, iminocoumarin derived heterocyclic compounds seem like a very interesting and unexplored scientific area for designing and preparing compounds with a broad potential for a variety of applications as optical materials. Most of the described iminocoumarins are substituted with an electron-donating group at positions 6 and/or 7 as well as an electron-accepting moiety at position 3, which caused the enhanced absorption and fluorescence intensities similar to those observed in analogous coumarin derivatives. A majority of synthesized iminocoumarins contains the electron-donating *N,N*-dialkylamino group at position 7, while a broader diversity of the electron-accepting moiety at position 3 was achieved, including the cyano and acyl groups, as well as some heterocyclic skeletons including the benzimidazole, benzoxazole or benzothiazole cores (Figure 1a-b) [26,27].

As an important feature, suchlike derivatives possess extended π -conjugation that leads to their improved spectral properties such as large Stokes shifts, enhanced fluorescence intensity or high quantum yields [28,29]. Interestingly, benzocoumarin and benzoiminocoumarin derivatives (known as *bent*-benzocoumarins) substituted with electron-donating *N,N*-diethylamino group and electron-accepting group such as 2-benzthiazolyl, 4-pyridyl or 4-pyridinium moiety at the opposite end of the

skeleton, have shown strong fluorescence in the solid state exhibiting the shape dependent emission (Figure 1c), while their precipitation offers highly fluorescent nanoparticles [30].

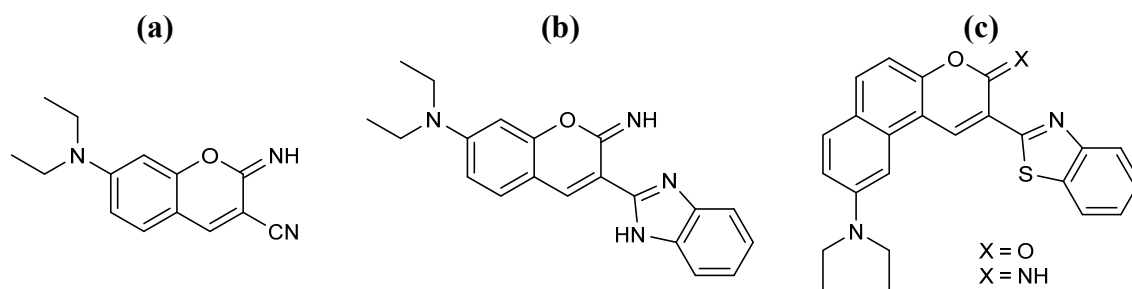


Figure 1. Structure of previously reported iminocoumarin derivatives.

Taking into account that nitrogen-containing heterocycles, among which benzazoles seems to be one of the most interesting and promising, represent an important class of organic subunits in the design of novel materials with a potential use in biomedical sciences as well as optical probes, we have devised novel iminocoumarin derivatives having an electron-accepting imidazo[4,5-*b*]pyridine nuclei at position 3, while bearing different substituents on the coumarin core. Furthermore, we have explored their spectral properties in several solvents of different polarities as well as acid-base properties for their potential application as optical pH indicators in solutions.

2. Experimental section

2.1. Chemistry

2.1.1. General Methods

From commercial available suppliers Aldrich, Acros and Fluka all chemicals and solvents were purchased. Using SMP11 Bibby apparatus, melting points were recorded and are not corrected. Using TMS as an internal standard as well as DMSO-*d*₆ solutions, the ¹H and ¹³C NMR spectra of newly prepared compounds were recorded on a Varian Bruker Avance III HD 400 MHz/54 mm Ascend, Bruker AV300 or Bruker AV600 spectrophotometer at 300, 400, 600, 150, 100 and 75 MHz respectively. Chemical shifts are reported in ppm (δ) relative to TMS. Within using thin layer chromatography with Merck silica gel 60F-254 plates all compounds were routinely checked while the spots were detected under UV light (254 nm). Column chromatography was performed on silica gel (0.063-0.2 mm) Fluka.

2.1.2. Synthesis of targeted compounds

2.1.2.1. *N*²-methylpyridine-2,3-diamine **2**

1.10 g (7.10 mmol) of *N*-methyl-3-nitropyridin-2-amine **1** and a solution of 13.3 g (60.00 mmol) SnCl₂·2H₂O in methanol (19 ml) and concentrated HCl (19 mL) were heated under reflux for 0.5 hours. After cooling, the reaction mixture was evaporated under vacuum and dissolved in water. The resulting solution was treated with 20% NaOH to pH = 14. The resulting precipitate was filtered off and filtrate was extracted with ethyl acetate. The organic layer was dried over anhydrous MgSO₄ and the solvent was evaporated under vacuum to give the product as purple oil (74%). ¹H NMR (DMSO-*d*₆, 600 MHz) δ/ppm = 7.38 (dd, 1H, *J*₁ = 4.95 Hz, *J*₂ = 1.53 Hz, H_{arom}), 6.65 (dd, 1H, *J*₁ = 7.35 Hz, *J*₂ = 1.53 Hz, H_{arom}), 6.32 (dd, 1H, *J*₁ = 7.32 Hz, *J*₂ = 1.53 Hz, H_{arom}), 5.54 (d, 1H, *J* = 4.20 Hz, NH), 4.59 (s, 2H, NH₂), 2.81 (d, 3H, *J* = 4.74 Hz, CH₃); ¹³C NMR (151 MHz, DMSO-*d*₆) δ/ppm = 148.58, 134.97, 130.25, 117.04, 111.99, 28.10. Anal. calcd. for C₆H₉N₃: C, 58.51; H, 7.37; N, 34.12. Found: C, 58.55; H, 7.37; N, 34.10%.

2.1.2.2. General method for preparation of compounds **4-5**

By heating a mixture of corresponding 2,3-diaminopyridine and ethyl cyanoacetate at 190 °C precursors **4-5** were prepared. After cooling on the room temperature, reaction mixture was treated with diethyl ether while resulting product was filtered off and recrystallized from ethanol [31].

2-(3-methyl-3*H*-imidazo[4,5-*b*]pyridin-2-yl)acetonitrile **4**

4 was prepared from **3** (0.58 g, 4.70 mmol) and ethyl cyanoacetate (0.75 mL, 7.10 mmol) after 45 min of heating to yield 0.42 g (46%) of brown powder; m.p. 146 °C. ¹H NMR (DMSO-*d*₆, 400 MHz): δ/ppm = 8.34 (dd, 1H, *J*₁ = 4.71 Hz, *J*₂ = 1.11 Hz, H_{arom}), 8.05 (1H, *J*₁ = 7.92 Hz, *J*₂ = 1.20 Hz, H_{arom}), 7.28 (1H, *J*₁ = 7.95 Hz, *J*₂ = 4.74 Hz, H_{arom}). 4.58 (s, 2H, CH₂), 3.75 (s, 3H, CH₃); ¹³C NMR (151 MHz, DMSO-*d*₆) δ/ppm = 148.10, 147.50, 143.53, 133.81, 126.66, 118.25, 115.84, 28.23, 17.95. Anal. calcd. For: C₉H₈N₄: C, 62.78; H, 4.68; N, 32.54. Found: C, 62.76; H, 4.69; N, 32.55%.

2-(3*H*-imidazo[4,5-*b*]pyridin-2-yl)acetonitrile **5**

5 was prepared from 2,3-diaminopyridine (1.0 g, 9.20 mmol) and ethyl cyanoacetate (1.5 mL, 13.70 mmol) after 30 min of heating to yield 0.6 g (40%) of brown powder; mp 268–271 °C. ¹H NMR (300 MHz, DMSO-*d*₆) δ/ppm = 13.06 (bs, 1H, NH), 8.34 (s, 1H, H_{arom}), 8.00 (s, 1H, H_{arom}), 7.25 (dd, 1H, *J*₁ = 8.03 Hz, *J*₂ = 4.79 Hz, H_{arom}), 4.42 (s, 2H, CH₂); ¹³C NMR (75 MHz, DMSO-*d*₆): δ/ppm = 143.73, 118.00 (2C), 116.17, 18.73. Anal. calcd. For: C₈H₆N₄: C, 60.75; H, 3.82; N, 35.42. Found: C, 60.79; H, 3.82; N, 35.41%.

2.1.2.3. General method for preparation of compounds 10-15

Ethanol solution (5 ml of absolute ethanol) of equimolar amounts of 2-cyanomethylimidazo[4,5-*b*]pyridines 4–5, corresponding aromatic aldehydes 6–9 and a few drops of piperidine, were stirred at the reflux for 2 hours. After cooling to room temperature, reaction mixture was filtered off. The products were purified by column chromatography on SiO₂ with dichloromethane/methanol as eluent.

4-nitro-2-(11-nitro-6H-chromeno[3,2-*e*]pyrido[3',2':4,5]imidazo[1,2-*c*]pyrimidin-6-yl)phenol 10

10 was prepared from **5** (0.20 g, 1.26 mmol) and **8** (0.21 g, 1.26 mmol) in absolute ethanol (5 mL) after refluxing for 2 hours to yield 0.01 g (1%) light yellow powder; m.p. 231-233 °C. ¹H NMR (600 MHz, DMSO) δ/ppm = 11.41 (bs, 1H, OH), 8.79 (d, 1H, *J* = 2.76 Hz, H_{arom}), 8.57 (s, 1H, H_{arom}), 8.36 (dd, 1H, *J*₁ = 9.06 Hz, *J*₂ = 2.82 Hz, H_{arom}), 8.25 (dd, 1H, *J*₁ = 4.68 Hz, *J*₂ = 1.38 Hz, H_{arom}), 8.15 (dd, 1H, *J*₁ = 8.10 Hz, *J*₂ = 1.38 Hz, H_{arom}), 8.09 (dd, 1H, *J*₁ = 9.00 Hz, *J*₂ = 2.88 Hz, H_{arom}), 7.64 (s, 1H, H_{arom}), 7.51 (d, 1H, *J* = 9.00 Hz, H_{arom}), 7.31 (dd, 1H, *J*₁ = 8.10 Hz, *J*₂ = 4.74 Hz, H_{arom}), 6.86 (d, 1H, *J* = 8.88 Hz, H_{arom}); ¹³C NMR (151 MHz, DMSO-*d*₆) δ/ppm = 156.69, 152.54, 145.70, 144.71, 144.65, 143.51, 139.24, 135.72, 127.26, 127.16, 127.13, 126.17, 125.27, 124.67, 119.83, 119.39, 117.19, 116.51, 114.10. MS (ESI): *m/z* = 457.04 ([*M*+1]⁺). Anal. calcd. for C₂₂H₁₂N₆O₆: C, 57.90; H, 2.65; N, 18.42; O, 21.03. Found: C, 58.02; H, 2.63; N, 18.39; O, 20.97.

3-(3H-imidazo[4,5-*b*]pyridin-2-yl)-6-methoxy-2H-chromen-2-imine 11

11 was prepared from **5** (0.20 g, 1.26 mmol) and **6** (0.19 g, 1.26 mmol) in absolute ethanol (5 mL) after refluxing for 2 hours to yield 0.08 g (21%) bright yellow powder in the form of tautomers in the ratio 1:3; m.p. 269-270 °C. ¹H NMR (300 MHz, DMSO): 12.91 (s, 1H, NH), 9.04 (s, 1H, H_{arom}), 8.39 (d, 1H, *J* = 3.54 Hz, H_{arom}), 8.08 (d, 1H, *J* = 7.92 Hz, H_{arom}), 7.55 (d, 1H, *J* = 2.61 Hz, H_{arom}), 7.49 (d, 1H, *J* = 9.06 Hz, H_{arom}), 7.34 (dd, 1H, *J*₁ = 9.05 Hz, *J*₂ = 2.87 Hz, H_{arom}), 7.26 (dd, 1H, *J*₁ = 7.90 Hz, *J*₂ = 4.72 Hz, H_{arom}), 3.86 (s, 3H, CH₃); ¹H NMR (300 MHz, DMSO): 12.74 (s, 1H, NH), 9.19 (s, 1H, H_{arom}), 8.44 (d, 1H, *J* = 3.54 Hz, H_{arom}), 8.03 (d, 1H, *J* = 7.92 Hz, H_{arom}), 7.63 (d, 1H, *J* = 2.61 Hz, H_{arom}), 7.49 (d, 1H, *J* = 9.06 Hz, H_{arom}), 7.34 (dd, 1H, *J*₁ = 9.05 Hz, *J*₂ = 2.87 Hz, H_{arom}), 7.26 (dd, 1H, *J*₁ = 7.90 Hz, *J*₂ = 4.72 Hz, H_{arom}), 3.86 (s, 3H, CH₃); ¹³C NMR (75 MHz, DMSO-*d*₆) δ/ppm = 155.99, 147.92, 144.67, 143.53, 121.15, 119.34, 118.34, 117.29, 111.60, 55.81. MS (ESI): *m/z* = 294.02 ([*M*+1]⁺). Anal. calcd. for C₁₆H₁₂N₄O₂: C, 65.75; H, 4.14; N, 19.17; O, 10.95. Found: C, 65.69; H, 4.09; N, 19.21; O, 10.90.

6-bromo-3-(3H-imidazo[4,5-*b*]pyridin-2-yl)-2H-chromen-2-imine 12

12 was prepared from **5** (0.20 g, 1.26 mmol) and **7** (0.25 g, 1.26 mmol) in absolute ethanol (5 mL) after refluxing for 2 hours to yield 0.024 g (6%) white crystals in the form of tautomers in the ratio

1:3; m.p. > 300 °C. ¹H NMR (300 MHz, DMSO) δ/ppm = 12.98 (s, 1H, H_{NH}), 9.03 (s, 1H, H_{arom}), 8.39 (d, 1H, *J* = 3.63 Hz, H_{arom}), 8.26 (s, 1H, H_{arom}), 8.11 (d, 1H, *J* = 7.62 Hz, H_{arom}), 7.88 (dd, 1H, *J*₁ = 8.82 Hz, *J*₂ = 2.16 Hz, H_{arom}), 7.52 (d, 1H, *J* = 8.82 Hz, H_{arom}), 7.30 (dd, 1H, *J*₁ = 7.92 Hz, *J*₂ = 4.71 Hz, H_{arom}); ¹H NMR (300 MHz, DMSO) δ/ppm = 12.77 (s, 1H, H_{NH}), 9.19 (s, 1H, H_{arom}), 8.45 (d, 1H, *J* = 3.60 Hz, H_{arom}), 8.32 (d, 1H, *J* = 1.98 Hz, H_{arom}), 8.03 (dd, 1H, H_{arom}), 7.88 (dd, 1H, *J*₁ = 8.82 Hz, *J*₂ = 2.16 Hz, H_{arom}), 7.52 (d, 1H, *J* = 8.82 Hz, H_{arom}), 7.27 (dd, 1H, *J*₁ = 7.92 Hz, *J*₂ = 4.71 Hz, H_{arom}), ¹³C NMR (75 MHz, DMSO-*d*₆) δ/ppm = 147.41, 144.96, 142.29, 135.52, 131.64, 127.01, 126.46, 120.82, 118.46, 117.21, 116.69. MS (ESI): *m/z* = 343.92 ([*M*+1]⁺). Anal. calcd. for C₁₅H₉BrN₄O: C, 52.81; H, 2.66; Br, 23.42; N, 16.42; O, 4.69. Found: C, 52.75; H, 2.70; Br, 23.41; N, 16.39; O, 4.72.

2-imino-3-(3-methyl-3H-imidazo[4,5-b]pyridin-2-yl)-2H-chromen-6-ol 13

13 was prepared from **4** (0.15 g, 0.87 mmol) and **9** (0.15 g, 0.87 mmol) in absolute ethanol (5 mL) after refluxing for 2 hours to yield 0.12 g (43%) yellow powder; m.p. 269-270 °C. ¹H NMR (300 MHz, DMSO) δ/ppm = 9.91 (s, 1H, OH), 8.55 (s, 1H, H_{arom}), 8.44 (dd, 1H, *J*₁ = 4.74 Hz, *J*₂ = 1.38 Hz, H_{arom}), 8.13 (dd, 1H, *J*₁ = 8.01 Hz, *J*₂ = 1.38 Hz, H_{arom}), 7.38 (m, 2H, H_{arom}), 7.20 (m, 2H, H_{arom}); ¹³C NMR (75 MHz, DMSO-*d*₆) δ/ppm = 154.16, 147.41, 144.19, 134.29, 127.03, 121.59, 119.05, 118.52, 118.29, 117.30, 113.20, 99.49, 29.66. MS (ESI): *m/z* = 294.02 ([*M*+1]⁺). Anal. calcd. for C₁₆H₁₂N₄O₂: C, 65.75; H, 4.14; N, 19.17; O, 10.95. Found: C, 65.80.; H, 4.13; N, 19.20; O, 11.00.

3-(3H-imidazo[4,5-b]pyridin-2-yl)-6-nitro-2H-chromen-2-imine 14

13 was prepared from **4** (0.06 g, 0.35 mmol) and **8** (0.05 g, 0.35 mmol) in absolute ethanol (5 mL) after refluxing for 2 hours to yield 0.08 g (81%) pale yellow powder; m.p. 293-294 °C. ¹H NMR (600 MHz, DMSO) δ/ppm = 8.93 (d, 1H, *J* = 2.76 Hz, H_{arom}), 8.78 (s, 1H, H_{arom}), 8.54 (dd, 1H, *J*₁ = 9.18 Hz, *J*₂ = 2.82 Hz, H_{arom}), 8.47 (dd, 1H, *J*₁ = 4.74 Hz, *J*₂ = 1.44 Hz, 1H), 8.17 (dd, 1H, *J*₁ = 7.98 Hz, *J*₂ = 1.44 Hz, H_{arom}), 7.78 (d, 1H, *J* = 9.18 Hz, H_{arom}), 7.38 (dd, 1H, *J*₁ = 8.04 Hz, *J*₂ = 4.80 Hz, H_{arom}), 3.84 (s, 3H, CH₃); ¹³C NMR (151 MHz, DMSO) δ/ppm = 157.04, 156.98, 148.27, 147.65, 145.58, 143.98, 143.26, 133.71, 127.12, 126.74, 124.66, 119.75, 118.39, 118.15, 117.38, 29.26. MS (ESI): *m/z* = 323.02 ([*M*+1]⁺). Anal. calcd. for C₁₆H₁₁N₅O₃: C, 59.81; H, 3.45; N, 21.80; O, 14.94. Found: C, 59.77; H, 3.42; N, 21.83; O, 15.01.

3-(3H-imidazo[4,5-b]pyridin-2-yl)-2-imino-2H-chromen-6-amine 15

0.04 g (0.12 mmol) of **14** was refluxed in a solution of 0.14 g (0.62 mmol) SnCl₂·2H₂O in methanol (3 ml) and concentrated HCl (1 mL) for 0.5 hours. After cooling, the reaction mixture was evaporated under vacuum and dissolved in water. The resulting solution was treated with 20% NaOH to pH = 14. The resulting precipitate was filtered off to yield 0.03 g (72%) of yellow powder: m.p. > 300 °C. ¹H

NMR (300 MHz, DMSO) δ /ppm = 8.48-8.40 (m, 2H, H_{arom}), 8.13 (dd, 1H, J_1 = 8.01 Hz, J_2 = 1.32 Hz, H_{arom}), 7.35 (dd, 1H, J_1 = 8.01 Hz, J_2 = 4.74 Hz, H_{arom}), 7.27 (d, 1H, J = 8.82 Hz, H_{arom}), 7.00 (dd, 1H, J_1 = 8.81 Hz, J_2 = 2.66 Hz, H_{arom}), 6.92 (d, 1H, J = 2.61 Hz, H_{arom}), 5.40 (s, 2H, NH₂), 3.79 (s, 3H, CH₃); ¹³C NMR (151 MHz, DMSO) δ /ppm = 158.80, 150.05, 148.22, 147.65, 146.12, 145.72, 144.09, 134.30, 126.97, 120.43, 118.87, 118.46, 117.82, 116.69, 110.53, 29.60. MS (ESI): m/z = 293.03 ([M+1]⁺). Anal. calcd. for C₁₆H₁₃N₅O: C, 65.97; H, 4.50; N, 24.04; O, 5.49. Found: C, 65.90; H, 4.49; N, 24.01; O, 5.51.

2.2. Spectroscopic characterization

UV-Vis absorption spectra were recorded in organic solvents of different polarities using Varian Cary 50 spectrophotometer in double-beam mode. Spectra were recorded in the range from 200–550 nm using 1 cm path quartz cells. Fluorescence measurements were recorded on Varian Cary Eclipse fluorescence spectrophotometer in quartz cells of 1 cm path length. Excitation maxima were determined from absorption spectra in the range of 200–500 nm. Emission spectra were recorded in the range from 400–600 nm and were corrected for the effects of time- and wavelength-dependent light-source fluctuations using a standard of rhodamine 101. The measurements were recorded in HPLC grade organic solvents (toluene, dioxane, diethyl ether, ethyl acetate, dichloromethane, acetonitrile, ethanol, methanol and water). Relative fluorescence quantum yields were determined using Miller's equation:

$$\phi_x = \phi_s \times A_s D_x n_x^2 / A_x D_s n_s^2$$

where A is the absorbance at the excitation wavelength, D is the area under the corrected emission curve, and n is the solvent refractive index. Subscripts s and x refer to standard and unknown, the former being quinine sulphate with a fluorescence quantum yield of 0.54.

2.3. pH titrations

Effect of pH on the spectroscopic properties was studied for all prepared iminocoumarins using UV-Vis spectroscopy. Additional testing was performed using fluorescence emission spectroscopy for compounds **11** and **12**. Spectra were recorded in solutions of universal buffers covering pH range from 1 to 13. Titrations were performed with 2×10^{-5} mol dm⁻³ solutions of **10–15** for absorbance and 1×10^{-6} mol dm⁻³ for the fluorescence measurements. For the curve fitting, a Boltzmann curve was used in the Origin software and the inflection point (x_0 parameter) was identified as the pK_a value.

2.4. Computational details

For ground state calculations, all molecular geometries were optimized with a very efficient B3LYP/6–31+G(d) model, which was designed to provide highly accurate thermodynamic and kinetic parameters for various organic systems, in line with our earlier work [32,33]. To account for the solvent effects, during geometry optimization, we included the implicit SMD solvation model corresponding to pure solvents [34]. Thermal corrections were extracted from the corresponding frequency calculations, so that all values pertain to Gibbs free energy differences at room temperature and normal pressure. The selection of such computational approach was motivated by its accuracy in evaluating the reaction parameters and pK_a values for a variety of analogous organic systems [35–37]. In this work, pK_a parameters were obtained in an absolute way using the proton's gas phase free energy of $G^\circ(H^+) = 6.28 \text{ kcal mol}^{-1}$ and its experimental aqueous solution solvation free energy of $\Delta G_{\text{SOLV}}(H^+) = -265.9 \text{ kcal mol}^{-1}$ [38], also employed by Truhlar and co-workers [34] in parameterizing the utilized SMD model. The latter value includes a constant term of $-1.89 \text{ kcal mol}^{-1}$ associated with the change in the free energy on moving from a gas-phase pressure of 1 atm to a liquid-phase concentration of 1 M.

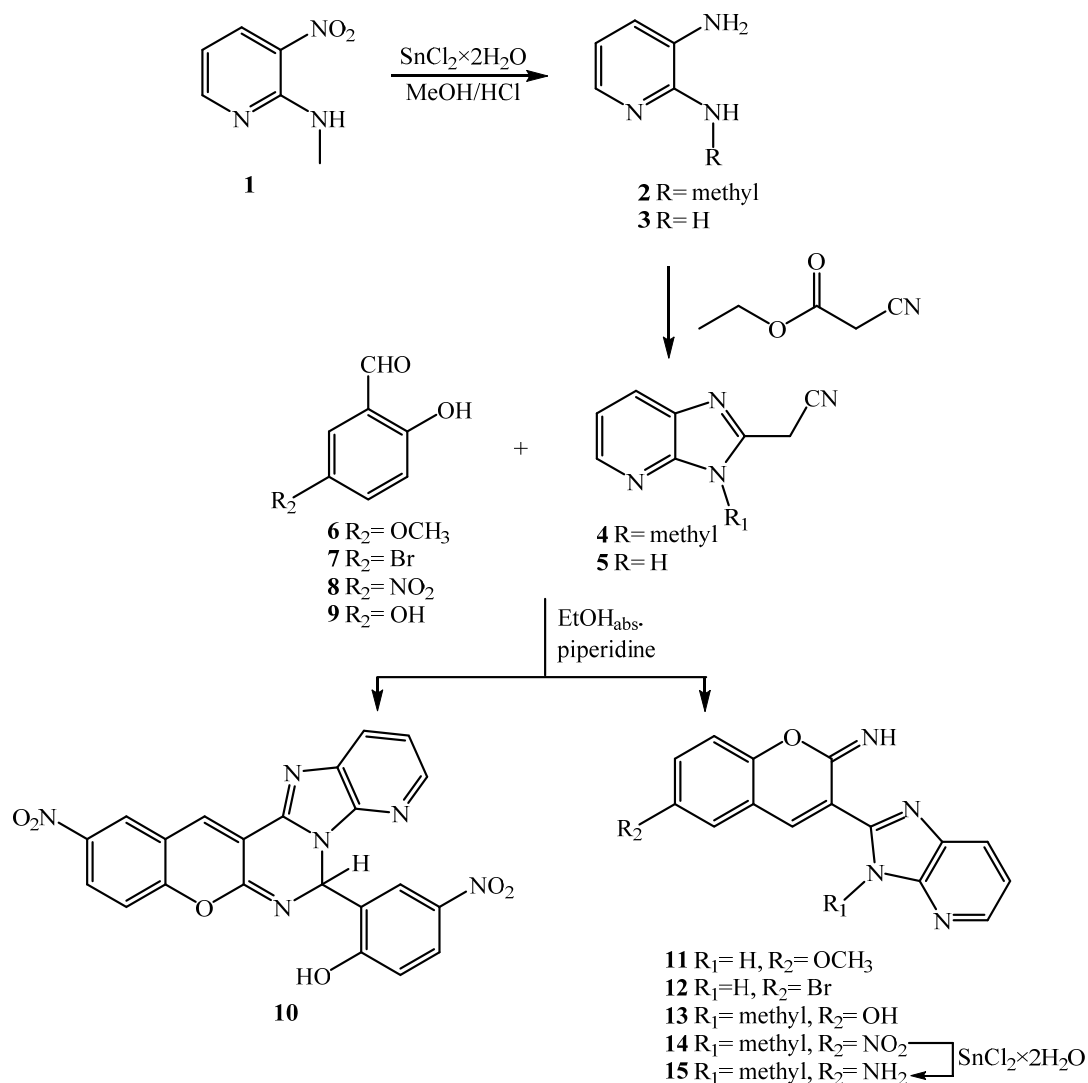
For excited state calculations, geometries of the ground and lowest excited states were optimized with DFT and time dependent DFT approaches, respectively, within the same (SMD)/B3LYP/6–31+G(d) model [39]. All calculations were performed with the Gaussian 16 package [40].

3. Results and Discussion

3.1. Chemistry

The synthesis of novel imidazo[4,5-*b*]pyridine derived iminocoumarins **11–15** is presented in Scheme 1 starting from *N*-methyl-2-nitroamino pyridine **1**. Within the classical reduction with $\text{SnCl}_2 \times 2\text{H}_2\text{O}$ in methanol, *N*-methyl-2,3-diaminopyridine **2** was prepared. Additionally, to prepare the main precursors for the synthesis of targeted iminocoumarins, namely, 2-cyanomethyl-*N*-substituted(unsubstituted) imidazo[4,5-*b*]pyridines **4–5**, the cyclocondensation of systems **2–3** was conducted with ethyl cyanoacetate [31]. Due to the condensation with 5-substituted salicylaldehydes **6–9**, the targeted imidazo[4,5-*b*]pyridine derived iminocoumarins **11–15** were prepared in low to moderate reaction yields after the purification through the column chromatography on silicagel with dichloromethane/methanol as an eluent. The substituents in the used 5-substituted salicylaldehydes **6–9** have proven to have a significant impact on the reaction yields. Thus, 5-bromo and 5-methoxy substituted salicylaldehydes gave targeted iminocoumarins in very low reaction yields (6 and 21%, respectively), while the highest yield has been observed when the 5-hydroxysalicylaldehyde was

employed (81%). Amino substituted **15** was prepared by the reduction with $\text{SnCl}_2 \times 2\text{H}_2\text{O}$ in methanol. Besides targeted **14**, the condensation reactions offered the pentacyclic product **10** from 5-nitrosalicylaldehyde, which was separated from nitro substituted **14** by the column chromatography on silicagel. Compounds **11** and **12** exist as a mixture of two inseparable tautomers which was confirmed by the ^1H NMR spectra in which the double signals were observed.



Scheme 1. Synthesis of imidazo[4,5-*b*]pyridine derived iminocoumarins **11–15**.

The structures of all newly prepared imidazo[4,5-*b*]pyridine derived iminocoumarins **11–15** as well as the cyclic derivative **10** were confirmed by the NMR spectroscopy and elemental analysis. Based on the chemical shifts in ^1H and ^{13}C NMR spectra, together with the values of H–H coupling constants in the ^1H spectra, the structure of all newly prepared derivatives was elucidated. Reduction of **1** was confirmed due to the presence of signal related to the amino H atoms. Furthermore, the existence of signals between 4.58–4.42 ppm related to the methylene group, together with the

disappearance of signals for amino protons, confirms the formation of the 2-cyanomethylimidazo[4,5-*b*]pyridine moiety in the structure of **4–5**. The reduction of nitro substituted iminocoumarin **14** was established by the observation of singlet related to the amino protons at the 5.40 ppm in the ^1H NMR spectra of **15**.

3.2. Spectroscopic characterization

To study the spectroscopic properties of the prepared compounds **10–15**, absorption and fluorescence emission spectra were recorded in several organic solvents of different polarities [41,42]. The main focus was to study the influence of the substituent placed both at the coumarin nuclei and the nitrogen atom of imidazo[4,5-*b*]pyridine core, as well as the impact of the solvent on spectroscopic features, which could be strongly influenced by the electronic nature of the introduced substituents and the polarity of the solvent. Optical properties of all studied compounds are presented in Table S1.

3.2.1. UV-Vis absorption spectra

In order to evaluate the impact of the solvent polarity on the spectroscopic characteristics of tested compounds, stock solutions were prepared in five polar and four non-polar solvents. UV-Vis spectra were taken at the same concentration of chromophores ($2 \times 10^{-5} \text{ mol dm}^{-3}$) in the range of 200–550 nm at room temperature, while employing solvents of a high purity grade with different $E_T(30)$ solvent polarity parameters. The absorption spectra of representative **10** and **11** are displayed in Figure 1, while for all other studied compounds in Figure S1.

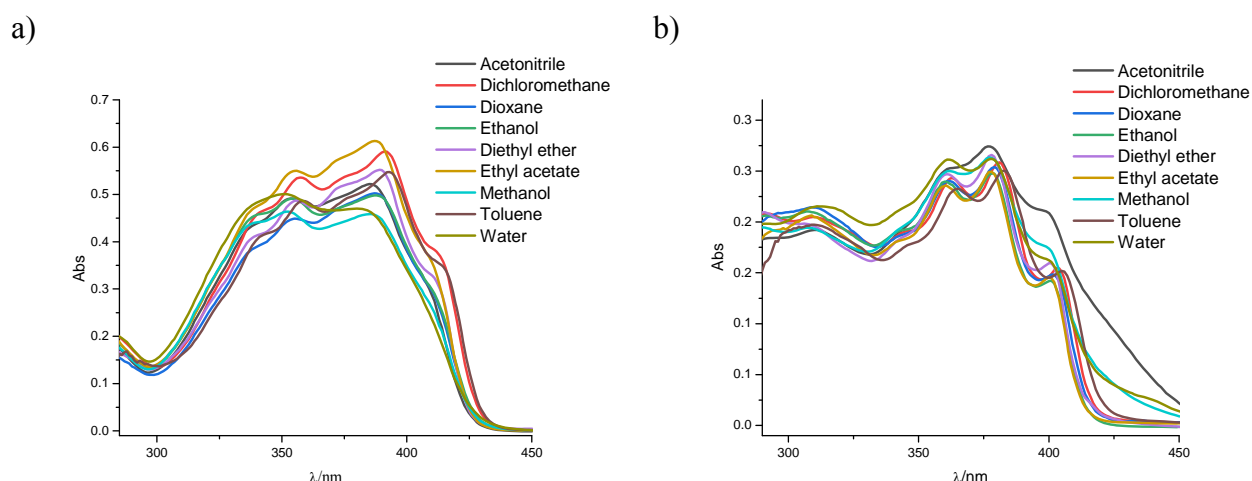


Figure 1. UV-Vis spectra of **11** (a) and **10** (b) at $c \approx 2 \times 10^{-5} \text{ mol dm}^{-3}$ in organic solvents of varying polarities.

When considering the absorption spectra of the methoxy substituted derivative **11**, the most intensive absorbance with a slight hyperchromic effect in comparison to all other solvents was observed in ethyl acetate, while in methanol the absorption spectra showed the hypochromic shift. In toluene, **11** showed slight bathochromic shift of absorption maxima relative to other solvents. Contrary to that, spectra taken in water revealed a slight hypsochromic shift. On the other hand, the absorption spectrum of cyclic **10** reveals the highest absorbance intensity in acetonitrile, while in ethyl acetate the spectral intensity displayed the hypochromic shift. The slight bathochromic shift of maxima can be observed in toluene. The recorded absorption spectra of tested compounds revealed that there is no significant impact of the solvents polarity on the absorption maxima and intensity.

3.2.2. Fluorescence emission spectra

Fluorescence emission spectra were recorded at the concentration of $1 \times 10^{-6} \text{ mol dm}^{-3}$ for **10** and **13–15**, and at the concentration $2 \times 10^{-7} \text{ mol dm}^{-3}$ for **11** and **12** due to differences in their solubility under employed conditions [43]. Excitation wavelengths were determined from the absorbance maxima and the spectra were not corrected for the inner filter effects. The emission spectra of representative derivatives **12** and **13** are shown in Figure 2, while in Figure S2 for other systems. Emission spectra of all compounds showed one emission band and one maxima in all solvents with the exception of **11** (Figure S2b) that showed two emission maxima in several solvents.

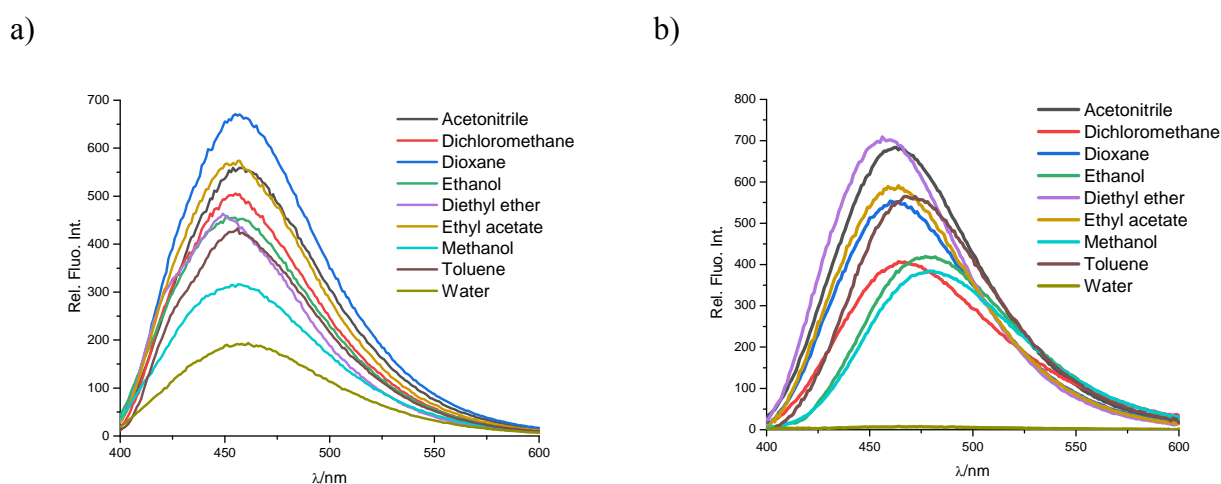


Figure 2. Emission spectra of **12** (a, $c = 2 \times 10^{-7} \text{ mol dm}^{-3}$, $\lambda_{\text{exc.}} = 385 \text{ nm}$) and **13** (b, $c = 1 \times 10^{-6} \text{ mol dm}^{-3}$, $\lambda_{\text{exc.}} = 312 \text{ nm}$) in organic solvents of varying polarities.

Emission spectra of **12** and **13** showed the strong impact of the solvent polarity on the fluorescence characteristics. In the most polar water solution, **12** showed significant hypochromic shift of fluorescence intensity, while **13** did not show any fluorescence. By decreasing the solvent polarity, **12**

revealed the hyperchromic effect. The strongest fluorescence intensity of **12** was demonstrated in dioxane with a slight hypsochromic shift relative to spectra taken in water (~ 5 nm). Compound **13** showed the bathochromic shift of emission maxima in methanol, ethanol and toluene when compared to all others solvents (~ 10 – 15 nm). The strongest hyperchromic effect of the intensity has been observed in diethyl ether with a slight hypsochromic effect. The strongest hypochromic effect with the significant decrease of the intensity has been observed in methanol. Figure 3 presents the comparison of spectra taken in one polar and one nonpolar solvent for compounds **10** and **13** (Figure 3a) whose spectra has been recorded at the same concentration 1×10^{-6} mol dm $^{-3}$ and excitation wavelength of 312 nm as well as spectra of compounds **11** and **12** (Figure 3b) recorded at the concentration 2×10^{-7} mol dm $^{-3}$ and excitation wavelength of 385 nm.

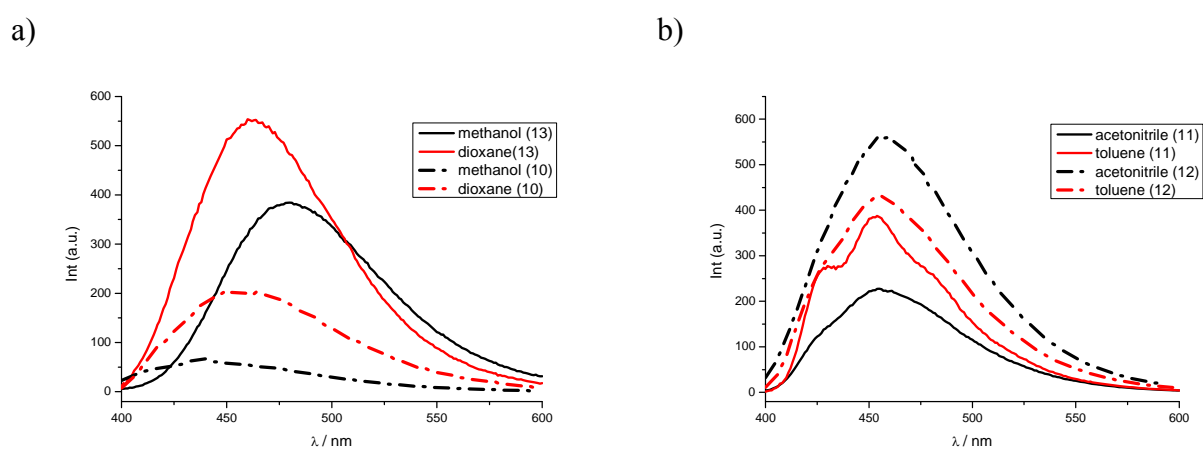


Figure 3. Compared emission spectra of **10** and **13** (a, $c = 1 \times 10^{-6}$ mol dm $^{-3}$, $\lambda_{exc.} = 312$ nm) and **11** and **12** (b, $c = 2 \times 10^{-7}$ mol dm $^{-3}$, $\lambda_{exc.} = 385$ nm) in one polar and one nonpolar organic solvent.

Pentacyclic derivative **10** revealed a strong hyperchromic effect of fluorescence intensity and a bathochromic shift of emission maxima in both polar (methanol) and nonpolar (dioxane) solvents, which is particularly pronounced in methanol relative to hydroxyl substituted **13**. Emission spectra taken for methoxy- **11** and bromo-substituted **12** revealed that the introduction of halogeno substituent increases the emission intensity in both polar (acetonitrile) and nonpolar (toluene) solvents. Compound **11** displayed two emission maxima in toluene, while in acetonitrile we observed a significant hypochromic effect of the fluorescence intensity.

Additionally, the quantum yields recorded in ethanol are very low for **10** (0.017), **13** (0.045), **14** (0.018) and **15** (0.026), and moderate for **11** (0.123), while are highest for the bromo-substituted derivative **12** (0.414). Furthermore, we observed a pronounced difference in the spectral properties of iminocoumarin fluorophores in chosen organic solvents and water, both in absorption and emission spectra which could be promising for their potential application as optical probes.

3.3. Experimental acid-base properties of studied iminocoumarin derivatives

In order to inspect the potential of prepared derivatives **10–15** as optical pH indicators, the influence of their spectroscopic properties relative to changes in the pH conditions was determined through the spectroscopic pH titrations [44,45]. To evaluate the acid-base features and characterize novel optical pH probes, we have determined the aqueous solution pK_a values from the obtained spectroscopic data [46], which relies on the optical determination of the concentrations of the acidic (HA) and basic forms (A^-) through the Henderson–Hasselbalch equation [47]:

$$pH = pK_a + \log \frac{[A^-]}{[HA]}$$

Lowering the pH conditions allowed the protonation of investigated compounds and the reorganization of the electron density within the cyclic units, which induced pronounced spectral changes in both absorption and emission spectra, thereby confirming the possible use of the studied compounds as pH optical probes (Fig. 4). Spectral properties upon pH titrations for **10–15** are presented in Table 1, while pH dependent absorption spectra for **10**, **13** and **15**, and emission spectra for **10**, **13** and **14** are deposited in the Supplementary information.

Table 1. Effect of pH on the absorption and emission properties of **10–15** in buffered aqueous solutions.

	λ_a (nm)			$\epsilon \times 10^3$ (dm ³ mol ⁻¹ cm ⁻¹)			λ_{em} (nm)			Stokes shift (nm)			pKa
	Acidic ^a	Neutral ^b	Basic ^c	Acidic	Neutral	Basic	Acidic	Neutral	Basic	Acidic	Neutral	Basic	
10	368 313	400 378 361 313	405 383 313	11.7 10.0	7.65 22.7 13.2 11.4	13.9 16.1 10.0	464	442	444	96	37	39	5.97
11	388 347	382 351	381 328	23.2 32.3	24.1 26.0	23.7 22.0	507	471	-	119	89	-	3.30 12.39
12	375 345	375	382 323	26.3 28.0	14.6	20.1 18.1	437	458	-	62	83	-	3.33
13	381 318	359 309	422 323 294	6.7 17.4	8.2 15.5	4.2 12.9 11.4	419	419	-	38	60	-	2.40
14	339 310 268	326 269	417 374 305	15.2 17.0 17.2	15.0 20.2	16.4 14.5 14.3	422	462	-	83	136	-	10.28
15	338 315	384 310	417 314	14.5 15.5	4.8 16.7	5.9 10.9	-	-	-	-	-	-	3.08

^a 0.1 M HCl; ^b MQ water; ^c buffer at pH = 13

As the spectra show, differences in the pH conditions resulted in significant spectral changes in both absorption and emission spectra. Specifically, these changes for **11** and **12** are more pronounced in the fluorescence spectra relative to their absorption spectra. For **11**, in acidic conditions, we observed the

small hypsochromic shift of the absorption maxima with a strong hyperchromic effect of the absorption intensity at 351 nm relative to the absorption spectra at pH 7.04 (Figure 4a). In basic conditions (pH = 12.93), we noticed the formation of novel absorption maxima at 328 nm.

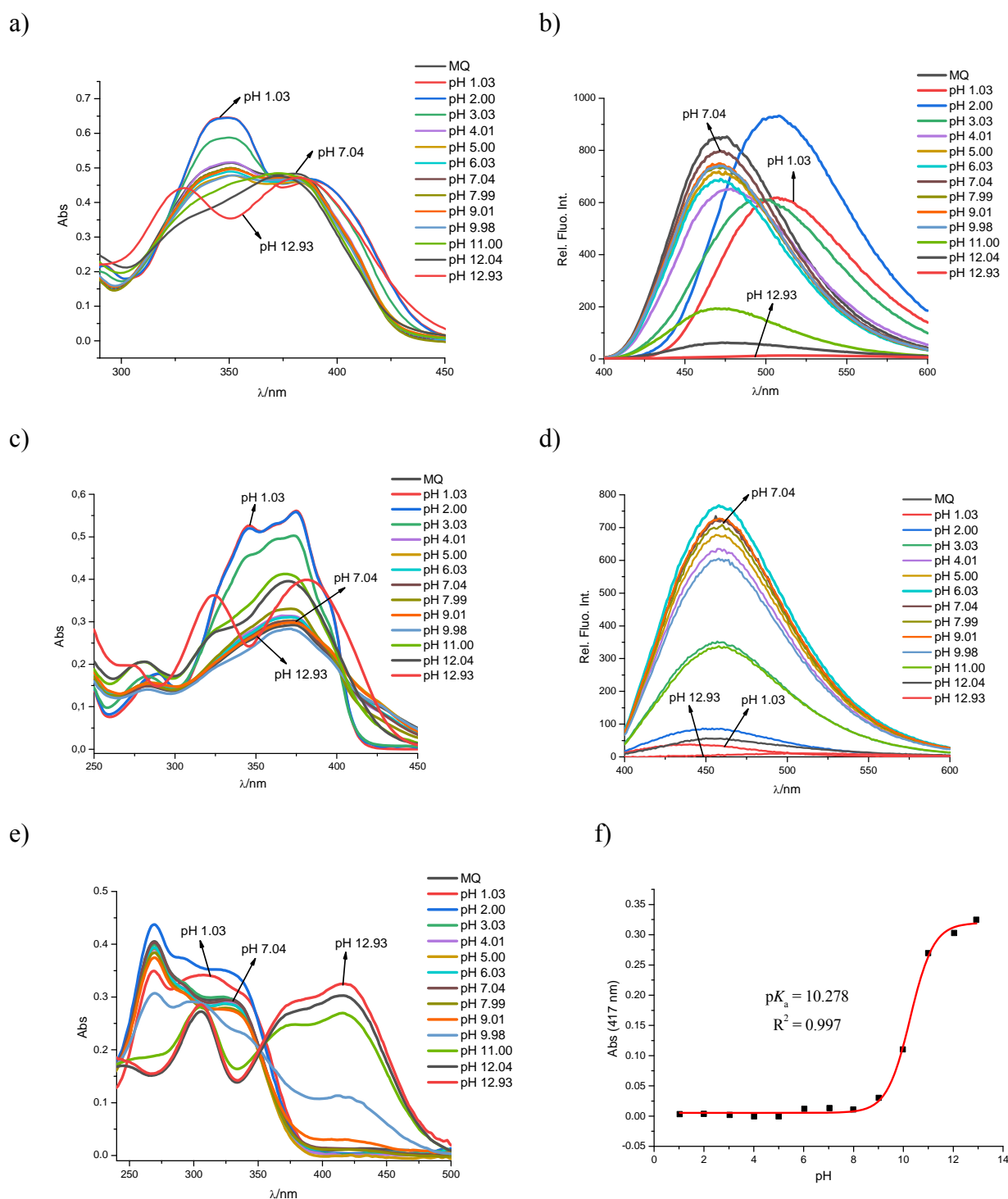


Figure 4. Absorption (a, c, e) and emission (b, d) spectra of **11**, **12** and **14** at different pH values in buffer ($\lambda_{exc(11)} = 380$ nm, $\lambda_{exc(12)} = 320$ nm); f) ratiometric absorption pH titration curve from which the pK_a for **14** was obtained by using a Boltzmann curve.

Furthermore, when the emission spectra for **11** (Figure 4b) at pH 7.04 is compared to that at pH 1.03, we observe that the protonation caused a significant bathochromic effect of maxima as well as hypochromic effect of the emission intensity. Under highly basic conditions at pH 12.93, we noticed an almost total quenching of fluorescence, in line with some earlier reports on similar derivatives [48]. On the other hand, data for **12** (Figure 4c) reveal the formation of novel absorption maxima at 345 nm in highly acidic media at pH 1.03, as well as a strong hyperchromic effect of absorption intensity at 375 nm. As with **11**, in strong basic conditions there is a formation of a novel absorption maximum at 323 nm as well as a small bathochromic and a significant hyperchromic shift of the second absorption maxima. In emission spectra (Figure 4d) at pH 12.93 one again observes an almost total quenching of the fluorescence for **12**, while in strong acidic conditions when compared to emission spectra taken at pH 7.04, we might observe a strong and significant hypochromic effect of the fluorescence intensity. Absorption spectra for **14** at pH 1.03 (Figure 4e) has shown the formation of one novel maxima at 310 nm with a small hyperchromic intensity shift at other two maxima. In strong basic conditions at pH 12.93, we observed the formation of novel two maxima at 417 and 374 nm with significant absorbance intensity, as well as one absorption maxima at 305 nm. Figure 5 presents the spectral changes for **11** under highly acidic (pH 1.03) and highly basic (pH 12.93) conditions.

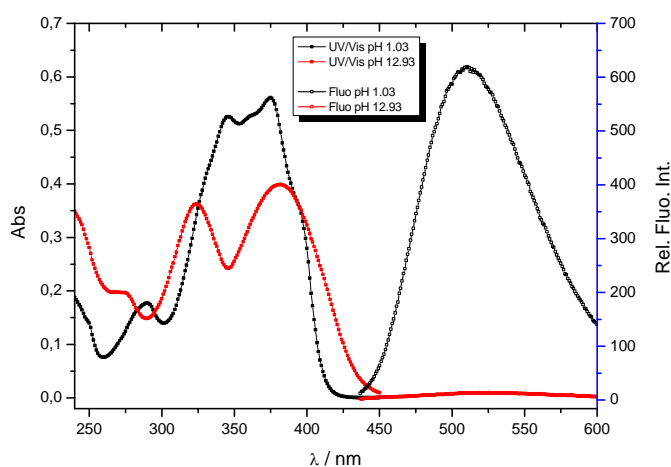


Figure 5. Typical absorption and fluorescence emission spectra of compound **11** ($\lambda_{\text{exc}} = 380 \text{ nm}$) in buffer at pH = 1.03 and pH = 12.93.

Additionally, as presented in Table 1, all compounds showed Stokes shifts from 38 to 136 nm indicating that in some compounds there is a large difference in the excitation energy, especially for **11** and **14**. The acid–base properties of studied compounds **10–15** are characterized by an 'apparent' pK_a value. Interestingly, while for all other compounds we elucidated a single pK_a value, **11** allowed the detection of two pK_a values, which means that this compound exist in three different pH sensitive forms under employed conditions that are spectrally detectable in solution, which is later confirmed by the computational analysis.

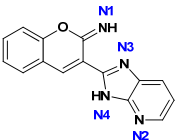
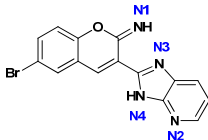
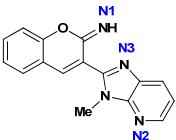
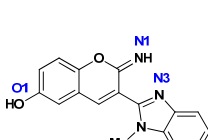
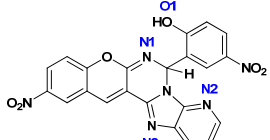
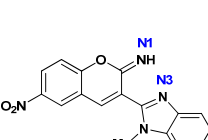
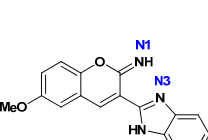
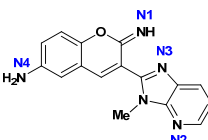
3.4. Computational analysis

Computational analysis was initiated to offer a further insight into the acid/base properties of studied derivatives and to relate them with the observed spectroscopic features in solution. Initially, we focused on calculating the pK_a values for systems **10–15** and two reference molecules **R1** and **R2** (Table 2), that will help us evaluate the effect of the introduced iminocoumarin substituents on the considered properties. Before proceeding with the analysis, let us emphasize an excellent agreement between calculated and measured data, evident in the absolute deviation of only 0.65 pK_a units for all seven experimentally determined pK_a constants, which confirms the validity of the employed computational approach and renders other computed values reliable as well.

Considered systems are composed of the iminocoumarin core and the imidazo[4,5-*b*]pyridine unit, connected to form an extended π -electron network. This notion helps rationalize significantly modified acid-base features in the prepared conjugates from those that each fragment exhibits when individually present. Specifically, in the least substituted **R1**, the most basic position is the iminocoumarin imine nitrogen (N1), having the pK_a value of 11.8, being considerably more basic than in related 2-quinolones where it is typically around 9 [49]. This suggests that in the aqueous solution, **R1** will predominantly exist as a cation monoprotated at the identified N1 atom. The next in line for the protonation is the pyridine nitrogen (N2) with $pK_a = 3.9$, a value which seems to contradict a usually superior basicity of imidazoles ($pK_a = 6.95$ for imidazole) over pyridines ($pK_a = 5.23$ for pyridine) [50,51]. The reason for that is the mentioned extended π -network, which depletes the electron density from the imidazo[4,5-*b*]pyridine moiety into the iminocoumarin unit, thereby reducing the basicity of both constituting fragments in **R1** and similar systems. This effect is, clearly, more pronounced for the imidazole ring, because of its vicinity to the iminocoumarin core, relative to a more distant pyridine. Nevertheless, the calculated basicity constant of $pK_a = 3.9$ for **R1**, allows the existence of dicationic **R1**⁺⁺ under highly acidic environment employed in this work ($1 < \text{pH} < 3.9$). Lastly, the utilized synthetic design drastically reduces the basicity of the imidazole fragment, being $pK_a = -7.2$ here, thus completely disfavoring its formation in our experiments.

Along these lines, the highest proton-releasing ability in **R1** resides on the imidazole amine, which is calculated at $pK_a = 20.1$, also being significantly less acidic than in the parent imidazole ($pK_a = 14.2$) [52], again due to its condensation with iminocoumarin. Taken all together, the calculated pK_a values indicate that within the employed conditions ($\text{pH} \approx 1\text{--}13$), **R1** exchanges through dicationic ($1 < \text{pH} < 3.9$), monocationic ($3.9 < \text{pH} < 11.8$) and neutral ($11.8 < \text{pH} < 13$) protonation forms, with two most basic sites being the iminocoumarin N1 and pyridine N2 nitrogen atoms (the entire acid-base equilibria is displayed in Figure S5).

Table 2. Calculated aqueous-phase pK_a values for studied systems at the (SMD)/B3LYP/6-31+G(d) level of theory. Experimental values determined in this work are given in square brackets for comparison. Shaded protonation states indicate the dominant protonation form at neutral pH = 7.

System	State	$pK_a(\text{calc})$	Protonation Reaction	System	State	$pK_a(\text{calc})$	Protonation Reaction
	$R1^{3+}$				12^{3+}		
	\uparrow	-7.2	$N3 \rightarrow N3^+$		\uparrow	-7.4	$N3 \rightarrow N3^+$
	$R1^{2+}$				\uparrow	3.8 [3.33]	$N2 \rightarrow N2^+$
	\uparrow	3.9	$N2 \rightarrow N2^+$		\uparrow	10.9	$N1 \rightarrow N1^+$
	$R1^+$				\uparrow	19.7	$N4^- \rightarrow N4$
	\uparrow	11.8	$N1 \rightarrow N1^+$		\downarrow	21.3	$N1^- \rightarrow N1$
\downarrow	20.1	$N4^- \rightarrow N4$	\downarrow				
\downarrow	22.6	$N1^- \rightarrow N1$	\downarrow				
$R1^{2-}$			12^{2-}				
	$R2^{3+}$				13^{3+}		
	\uparrow	-4.0	$N3 \rightarrow N3^+$		\uparrow	-3.9	$N3 \rightarrow N3^+$
	$R2^{2+}$				\uparrow	4.0 [2.40]	$N2 \rightarrow N2^+$
	\uparrow	3.9	$N2 \rightarrow N2^+$		13^+		
	$R2^+$				\uparrow	12.7	$N1 \rightarrow N1^+$
	\uparrow	12.3	$N1 \rightarrow N1^+$		\downarrow	13.9	$O1^- \rightarrow O1$
\downarrow	20.9	$N1^- \rightarrow N1$	\downarrow	26.9	$N1^- \rightarrow N1$		
$R2^-$			13^-				
	10^{3+}				14^{3+}		
	\uparrow	-26.9	$O1 \rightarrow O1^+$		\uparrow	-4.6	$N3 \rightarrow N3^+$
	10^{2+}				\uparrow	3.4	$N2 \rightarrow N2^+$
	\uparrow	-4.5	$N2 \rightarrow N2^+$		14^+		
	10^+				\uparrow	10.4 [10.28]	$N1 \rightarrow N1^+$
	\uparrow	1.2	$N1 \rightarrow N1^+$		\downarrow	14.1	$N1^- \rightarrow N1$
\downarrow	5.9 [5.97]	$N3 \rightarrow N3^+$	14^-				
\downarrow	9.7	$O1^- \rightarrow O1$	\downarrow				
10^{2-}			14^-				
	11^{3+}				15^{3+}		
	\uparrow	-11.1	$N3 \rightarrow N3^+$		\uparrow	-0.8	$N4 \rightarrow N4^+$
	11^{2+}				\uparrow	4.4 [3.08]	$N2 \rightarrow N2^+$
	\uparrow	4.1 [3.30]	$N2 \rightarrow N2^+$		15^+		
	11^+				\uparrow	13.7	$N1 \rightarrow N1^+$
	\uparrow	12.2 [12.39]	$N1 \rightarrow N1^+$		\downarrow	23.2	$N1^- \rightarrow N1$
\downarrow	20.1	$N4^- \rightarrow N4$	15^-				
\downarrow	24.8	$N1^- \rightarrow N1$					
11^{2-}							

As expected, the introduction of the imidazole *N*-methyl group in **R2**, increases the basicity of both iminocoumarin N1 and imidazole N3 sites, and the effect is 0.5 and 3.2 pK_a units, respectively. Interestingly, the basicity of the pyridine N2 nitrogen remains intact at $pK_a = 3.9$, suggesting practically no electronic interactions between directly annelated imidazole and pyridine. In addition, the acidity of the iminocoumarin N1 site is also enhanced in **R2**, by 1.7 pK_a units, yet still not bringing this process ($pK_a = 20.9$) within any reach of the employed experimental conditions. Nevertheless, the imidazole *N*-methylation does not change the fact that the relevant three protonation forms can be

analogously identified, with the corresponding transitions diprotonated \rightarrow monoprotoneated \rightarrow neutral in **R2** occurring at the pH values of 3.9 and 12.3, respectively.

In the systems evaluated in this work, we notice that, relative to **R1**, the introduction of the electron-donating $-\text{OMe}$ group enhances the basicity of iminocoumarin N1 in **11**, while electron-accepting $-\text{Br}$ reduces it in **12**. In both cases, the effect is small, 0.4 $\text{p}K_{\text{a}}$ units for $-\text{OMe}$ and 0.9 $\text{p}K_{\text{a}}$ units for $-\text{Br}$, which is justified through their significant distance from the protonation centre. Because of the same reason, the basicity of the pyridine N2 site remains practically intact at $\text{p}K_{\text{a}} = 4.1$ for **11** and $\text{p}K_{\text{a}} = 3.8$ for **12**, yet also confirming a subtle relation between the electronic features of the substituent and the resulting basicity, when related with the $\text{p}K_{\text{a}} = 3.9$ in the unsubstituted **R1**. When much stronger electron-donating groups are introduced on the iminocoumarin core, coupled with the imidazole *N*-methylation, $-\text{OH}$ group in **13** and, especially, $-\text{NH}_2$ group in **15**, the resulting $\text{p}K_{\text{a}}$ constants for the N1 and N2 protonations experience a larger increase. This underlines **15** as the most basic compound evaluated here, where the corresponding changes in the protonation forms occur at highest pH values, being linked with the $\text{p}K_{\text{a}}$ values of 4.4 and 13.7 for the N2 and N1 sites, respectively. With this in mind, it comes to a little surprise that **14**, containing one of the most potent electron-withdrawing nitro groups, belongs to the other side of the spectra, revealing the matching transitions between the protonation forms at lowest $\text{p}K_{\text{a}}$ values of 3.4 and 10.4 for the N2 and N1 sites, in the same order.

In concluding this part, we can underline that the employed synthetic strategy in preparing the targeted derivatives turned out very useful in designing potent pH probes, since their acid-base features can be significantly tuned with only a single substitution on the iminocoumarin core. Specifically, through a careful selection of the electron-donating or electron-withdrawing fragments, coupled with the imidazole *N*-methylation, one allows the changes in the protonation forms and the subsequent photophysical responses, to occur within a very narrow but focused range of pH values, which can easily be harnessed for their potential application. Precisely, among five selected derivatives **11–15**, the transition from monoprotoneated to diprotonated forms takes place between pH values of 3.4 (in **14**) and 4.4 (in **15**), while that from monoprotoneated to neutral ones occurs between pH values of 10.4 (in **14**) and 13.7 (in **15**), covering a somewhat broader range. Therefore, we can state that the considered systems show a notable promise to be employed as pH sensing molecules for monitoring changes in the aqueous-phase pH conditions from highly acidic to highly basic environments.

Lastly, when a more complex system **10** is concerned, the calculated $\text{p}K_{\text{a}}$ values identify four protonation forms that can be expected within the used experimental conditions. Due to the encapsulation within the six-membered ring, the basicity of the iminocoumarin N1 nitrogen is significantly lowered to $\text{p}K_{\text{a}} = 1.2$, yet still allowing fractions of this protonation form under lowest

considered pH conditions. Yet, its basicity is surpassed by the imidazole N3 nitrogen, which, in **10**, exceeds that of the pyridine nitrogen and assumes $pK_a = 5.9$, being in excellent agreement with the experimentally determined value of 5.97. All of this indicates that, unlike **11–15**, under neutral conditions, system **10** will predominantly exist as a neutral unionized molecule. As a further notable difference, the presence of the hydroxyl group in **10** allows deprotonation at $pK_a = 9.7$ and the existence of monoanionic **10**[−] at elevated pH conditions. Interestingly, despite being linked with the highly acidifying *p*-nitro group, the acidity of this −OH group matches that of phenol ($pK_a = 9.99$) [53]. Yet, it would likely be closer to the acidity of *p*-nitrophenol ($pK_a = 7.16$) [54] if it was not for the O1–H⋯N1 hydrogen bond in neutral **10** with $d(\text{O1–N1}) = 2.71 \text{ \AA}$ and $a(\text{O1–H–N1}) = 142.0^\circ$, which stabilizes the hydroxyl group and prevents a more efficient deprotonation. On the overall, the utilized conditions ($\text{pH} \approx 1\text{--}13$) allow **10** to change from diprotonated to monoanionic forms, which rationalizes a complex appearance of the electronic spectra for this conjugate (Figure S3).

In order to additionally evaluate the validity of the calculated pK_a values and confirm that experimentally observed photophysical responses are brought about by changes in the protonation forms of investigated derivatives, we have calculated UV-Vis absorption spectra for different protonation forms of **10–15** (Figures S6–S11), which reveal a very good agreement with experiments. If system **11** is considered as a representative case, the calculations nicely reproduce the hypsochromic shift of the absorption maxima and a hyperchromic effect of the absorption intensity at 351 nm (Figure S6) on going from monocationic **11**⁺ (neutral pH) towards dicationic **11**⁺⁺ form ($\text{pH} \approx 1$). In addition, calculations for unionized **11** ($\text{pH} \approx 13$) agree with the formation of a new absorption maximum at 328 nm, yet being somewhat shifted towards higher excitation energies in the calculated spectra. On the other hand, a much better quantitative agreement in the position of the absorption maxima is achieved in reproducing the formation of a novel band at 345 and 310 nm in a highly acidic media for **12**⁺⁺ and **14**⁺⁺, respectively, and a hyperchromic effect in both absorption intensities relative to their monocationic species at neutral pH. Lastly, the computed UV-Vis spectra for monoanionic **11**[−] suggest a further bathochromic shift of the absorption maxima and a small hyperchromic effect in the absorption intensity (Figure S6). The latter is not evident in experimentally measured spectra (Figure 4), thereby ruling out the existence of this protonation form in solution, being fully in line with the calculated $pK_a = 20.1$ that exceeds beyond the reach of utilized experimental conditions. Along these lines, the same kind of conclusions can be drawn for other systems as well, therefore suggesting that the calculated absorption spectra support the pH-dependent chemical speciation established by the computed thermodynamic acid-base constants.

4. Conclusions

We have described the synthesis and structural characterization of five novel imidazo[4,5-*b*]pyridine derived iminocoumarins **11–15** and one cyclic compound **10**, and presented their potential as optical probes for detecting pH changes in solution. The spectroscopic characterization of all compounds has been carried out using UV-Vis and fluorescence spectroscopies in nine solvents with different polarities. Obtained results revealed that the solvent polarity has a significant impact on the spectral characteristics for both absorption and emission spectra, while the type of the substituents placed either at the coumarin nuclei or the imidazo[4,5-*b*]pyridine amine nitrogen strongly influenced their photophysical features. The highest quantum yield has been recorded for the bromo-substituted iminocoumarin **12** (0.414).

The potential of studied compounds as optical pH indicators was determined through absorption and emission pH titrations employed in aqueous buffers with different pH values. The results demonstrated that modified pH conditions show an important influence on the recorded spectral changes. This was confirmed by experimentally determined aqueous solution pK_a values and further supported through DFT calculations, which achieved excellent agreement with measured values. Both sets of data strongly point out that compounds **11–15** highlight a useful strategy towards potent pH probes, since their acid-base features can be significantly modulated with only a single substitution on the iminocoumarin core. Specifically, all compounds are monocationic systems under neutral conditions, whereas their transition to diprotonated forms occurs at pH values between 3.4 and 4.4, while can be reverted to neutral unionized molecules at pH values between 10.4 and 13.7, thereby allowing a simple way to tune their spectral responses for a specific application [55].

Supplementary Materials: Figure S1: UV absorption spectra for systems **12–15**. Figure S2: Fluorescence emission spectra for systems **10–11** and **14–15**. Figure S3: UV pH titrations for systems **10**, **13** and **15**. Figure S4: Fluorescence pH titrations for systems **10**, **13** and **14**. Figure S5: Acid-base equilibria for system **R1**. Figures S6–S11: Calculated aqueous solution UV-Vis spectra for systems **10–15**. Figures S12-S29: NMR spectra of compounds **10–15**.

Author Contributions: **Ida Boček:** Conceptualization, Formal analysis, Investigation, Writing - Original Draft; **Marijana Hranjec:** Conceptualization, Formal analysis, Investigation, Writing - Original Draft, Writing - Review & Editing, Supervision; **Robert Vianello:** Formal analysis, Investigation, Writing - Original Draft, Writing - Review & Editing, Funding acquisition. All authors read and approved the final manuscript.

Funding: This work was supported by the Croatian Science Foundation under the grant number IP–2020–02–8090, which is gratefully acknowledged.

Declaration of Interest: The authors declare no conflict of interest.

References

- [1] H. Li, L. Cai, Z. Chen, Coumarin-derived fluorescent chemosensors, *Advances in Chemical Sensors*, Wang W (Ed.) InTech; 2011. pp. 121–150.
- [2] B.D. Wagner, The use of coumarins as environmentally-sensitive fluorescent probes of heterogeneous inclusion systems, *Molecules* (2009) 14 210–37. <https://doi.org/10.3390/molecules14010210>
- [3] L. Xie, Y. Chen, W. Wu, H. Guo, J. Zhao, X. Yu, Fluorescent coumarin derivatives with large stokes shift, dual emission and solid state luminescent properties: An experimental and theoretical study; *Dyes Pigm.* (2012) 92 1361–1369. <https://doi.org/10.1016/j.dyepig.2011.09.023>
- [4] G. Zhang, H. Zheng, M. Guo, L. Du, G. Liu, P. Wang, Synthesis of polymeric fluorescent brightener based on coumarin and its performances on paper as light stabilizer, fluorescent brightener and surface sizing agent, *Appl. Surf. Sci.* (2016) 367 167–173. <https://doi.org/10.1016/j.apsusc.2016.01.110>
- [5] G. Zhang, H. Zheng, G. Liu, P. Wang, R. Xiang, Synthesis and application of a multifunctional fluorescent polymer based on coumarin, *Bioresources* 11 (2016) 373–384. <https://doi.org/10.15376/biores.11.1.373-384>
- [6] R. Sánchez-de-Armas, M.Á. San Miguel, J. Oviedo, J.F. Sanz, Coumarin derivatives for dye sensitized solar cells: a TD-DFT study, *Phys. Chem. Chem. Phys.* 14 (2012) 225–233. <https://doi.org/10.1039/C1CP22058F>
- [7] K.D. Seo, I.T. Choi, Y.G. Park, S. Kang, J.Y. Lee, H.K. Kim, Novel D-A- π -A coumarin dyes containing low band-gap chromophores for dye-sensitised solar cells, *Dyes Pigm.* 94 (2012) 469–474. <https://doi.org/10.1016/j.dyepig.2011.01.009>
- [8] P. Wlodarczyk, S. Komarneni, R. Roy, W.B. White, Enhanced fluorescence of coumarin laser dye in the restricted geometry of a porous nanocomposite, *J. Mater. Chem.* 6 (1996) 1967–1969. <https://doi.org/10.1039/JM9960601967>
- [9] C. Ranjith, K.K. Vijayan, V.K. Praveen, N.S.S. Kumar, Photophysical investigation of 3-substituted 4-alkyl and/or 7-acetoxy coumarin derivatives—a study of the effect of substituents on

fluorescence, *Spectrochim. Acta A Mol. Biomol. Spectrosc.* 75 (2010) 1610–1616.
<https://doi.org/10.1016/j.saa.2010.02.027>

[10] A.R. Jagtap, V.S. Satam, R.N. Rajule, V.R. Kanetkar, The synthesis and characterization of novel coumarin dyes derived from 1,4-diethyl-1,2,3,4-tetrahydro-7-hydroxyquinoxalin-6-carboxaldehyde, *Dyes Pigm.* 82 (2009) 84–89. <https://doi.org/10.1016/j.dyepig.2008.11.007>

[11] A. Rabahi, M. Makhloufi-Chebli, S.M. Hamdi, A.M.S. Silva, D. Kheffache, B. Boutemur-Kheddis, M. Hamdi, Synthesis and optical properties of coumarins and iminocoumarins: Estimation of ground- and excited-state dipole moments from a solvatochromic shift and theoretical methods, *J. Mol. Liq.* 195 (2014) 240–247. <https://doi.org/10.1016/j.molliq.2014.02.029>

[12] O.W. Morawski, Ł. Kielesiński, D.T. Gryko, A.L. Sobolewski, O.W. Morawski, Highly Polarized Coumarin Derivatives Revisited: Solvent-Controlled Competition Between Proton-Coupled Electron Transfer and Twisted Intramolecular Charge Transfer, *Chem. Eur. J.* 26 (2020) 7281–7291. <https://doi.org/10.1002/chem.202001079>

[13] A. Shabbir, T. Jang, G. Lee, Y. Pang, Intramolecular charge transfer of coumarin dyes confined in *methanol-in-oil* reverse micelles, *J. Mol. Liq.* 346 (2022) 118313. <https://doi.org/10.1016/j.molliq.2021.118313>

[14] H. Xu, Y. Bu, J. Wang, M. Qu, J. Zhang, X. Zhu, G. Liu, Z. Wu, G. Chen, H. Zhou, A convenient fluorescent probe for monitoring lysosomal pH change and imaging mitophagy in living cells, *Sens. Actuators B Chem.* 330 (2021) 129363. <https://doi.org/10.1016/j.snb.2020.129363>

[15] H. Kim, S. Sarkar, M. Nandy, K.H. Ahn, Imidazolyl–benzocoumarins as ratiometric fluorescence probes for biologically extreme acidity, *Spectrochim. Acta A Mol. Biomol. Spectrosc.* 248 (2021) doi: 10.1016/j.saa.2020.119088

[16] C. Yoshikawa, H. Ishida, N. Ohashi, T. Itoh, Synthesis of a Coumarin-Based PPAR Fluorescence Probe for Competitive Binding Assay, *Int. J. Mol. Sci.* 22 (2021) 4034. <https://doi.org/10.3390/ijms22084034>

[17] A.A. Atta-Eyison, Performance Evaluation of Fluorescence and Photostability of Coumarin Disperse Yellow 82, *J. Chem. Eng. Mater. Sci.* 8 (2020) 11-19. <https://doi.org/10.4236/msce.2020.81002>

[18] H. M. Elaryian, M. A. Bedair, A. H. Bedair, R. M. Aboushahba, A. E.-A. S. Fouda, Synthesis, characterization of novel coumarin dyes as corrosion inhibitors for mild steel in acidic environment: Experimental, theoretical, and biological studies, *J. Mol. Liq.* 346 (2022) 118310. <https://doi.org/10.1016/j.molliq.2021.118310>

- [19] A.A. Bhagwat, K.C. Avhad, D.S. Patil, S. Nagaiyan, Design and Synthesis of Coumarin-Imidazole Hybrid Chromophores: Solvatochromism, Acidochromism and Non-Linear Optical Properties, *Photochem. Photobiol.* 95 (2018) 740-754. <https://doi.org/10.1111/php.13024>
- [20] H. Turki, S. Abid, S. Fery-Forgues, R. El Gharbi, Optical properties of new fluorescent iminocoumarins: Part 1, *Dyes Pigm.* 73 (2007) 311–316. <https://doi.org/10.1016/j.dyepig.2006.01.001>
- [21] U.S. Raikar, C.G. Renuka, Y.F. Nadaf, B.G. Mulimani, A.M. Karguppikar, M.K. Soudagar, Solvent effects on the absorption and fluorescence spectra of coumarins 6 and 7 molecules: Determination of ground and excited state dipole moment, *Spectrochim Acta A Mol Biomol Spectrosc* 65 (2006) 673–677. <https://doi.org/10.1016/j.saa.2005.12.028>
- [22] K. Khemakhem, H. Ammar, S. Abid, R. El Gharbi, S. Fery-Forgues Spectroscopic study of 3-aryl-7-methoxy-coumarin, iminocoumarin and bisiminocoumarin derivatives in solution. *Dyes Pigm.* 99 (2013) 594–598. <https://doi.org/10.1016/j.dyepig.2013.06.003>
- [23] D. Kim, Q.P. Xuan, H. Moon, Y.W. Jun, K.H. Ahn, Synthesis of Benzocoumarins and Characterization of Their Photophysical Properties, *Asian J. Org. Chem.* 3 (2014) 1089–1096. <https://doi.org/10.1002/ajoc.201402107>
- [24] K.C. Avhad, D.S. Patil, Y.K.C. Gawale, M.C. Subramaniyan Sreenath, I.H. Joe, N. Sekar, Large Stokes Shifted Far-Red to NIR-Emitting D- π -A Coumarins: Combined Synthesis, Experimental, and Computational Investigation of Spectroscopic and Non-Linear Optical Properties, *ChemistrySelect* 3(16) (2018) 4393–4405. <https://doi.org/10.1002/slct.201800063>
- [25] M. Fakhfakh, H. Turki, S. Fery-Forgues, R. El Gharbi, The synthesis and optical properties of novel fluorescent iminocoumarins and bis-iminocoumarins: Investigations in the series of urea derivatives, *Dyes and Pigments* 84 (2010) 108–113. <https://doi.org/10.1016/j.dyepig.2009.07.003>
- [26] N. Abid-Jarraya, K. Khemakhem, H. Turki-Guermazi, S. Abid, N. Saffon, S. Fery-Forgues, Solid-state fluorescence properties of small iminocoumarin derivatives and their analogues in the coumarin series, *Dyes and Pigments* 132 (2016) 177–184. <https://doi.org/10.1016/j.dyepig.2016.04.039>
- [27] S.B. Chemate, N. Sekar, Novel Iminocoumarin Derivatives: Synthesis, Spectroscopic and Computational Studies, *J. Fluoresc.*, 25 (2015) 1615–1628. <https://doi.org/10.1007/s10895-015-1648-4>
- [28] B. Hohl, E. Má dai, D. Boda, M. Valiskó, Modeling of a pH-tunable dual-response nanopore sensor, *J. Mol. Liq.* 310 (2020) 112946. <https://doi.org/10.1016/j.molliq.2020.112946>

- [29] S. Gurusamy, K. Krishnaveni, M. Sankarganesh, V. Sathish, P. Thanasekaran, A. Mathavan, Multiple target detection and binding properties of naphthalene-derived Schiff-base chemosensor, *J. Mol. Liq.* 325 (2021) 115190. <https://doi.org/10.1016/j.molliq.2020.115190>
- [30] M. Dai, S. Sarkar, C.W. Song, Y.J. Reo, Y.J. Yang, K.H. Ahn, Bent-Benzocoumarin Dyes that Fluoresce in Solution and in Solid State and Their Application to Bioimaging, *ChemPhotoChem* 4 (2020) 721–728. <https://doi.org/10.1002/cptc.202000059>
- [31] B. Lončar, N. Perin, M. Mioč, I. Boček, L. Grgić, M. Kralj, S. Tomić, M. Radić Stojković, M. Hranjec, Novel amino substituted tetracyclic imidazo[4,5-*b*]pyridine derivatives: Design, synthesis, antiproliferative activity and DNA/RNA binding study, *Eur. J. Med. Chem.* 217(5) (2021) 113342. <https://doi.org/10.1016/j.ejmech.2021.113342>
- [32] E. Horak, D. Babić, R. Vianello, N. Perin, M. Hranjec, I. Murković Steinberg, Photophysical properties and immobilisation of fluorescent pH responsive aminated benzimidazo[1,2-*a*]quinoline-6-carbonitriles, *Spectrochimica Acta Part A: Molecular and Biomolecular Spectroscopy* 227 (2020) 117588. <https://doi.org/10.1016/j.saa.2019.117588>
- [33] E. Horak, M. Hranjec, R. Vianello, I. Murković Steinberg, Reversible pH switchable aggregation-induced emission of self-assembled benzimidazole-based acrylonitrile dye in aqueous solution, *Dyes and Pigments* 142 (2017) 108–115. <https://doi.org/10.1016/j.dyepig.2017.03.021>
- [34] A.V. Marenich, C.J. Cramer, D.G. Truhlar, Universal solvation model based on solute electron density and on a continuum model of the solvent defined by the bulk dielectric constant and atomic surface tensions, *J. Phys. Chem. B* 113 (2009) 6378–6396. <https://doi.org/10.1021/jp810292n>
- [35] L. Hok, R. Vianello, Direct metal-free transformation of alkynes to nitriles: Computational evidence for the precise reaction mechanism, *Int. J. Mol. Sci.* 22 (2021) 3193. <https://doi.org/10.3390/ijms22063193>
- [36] G.J. Rowlands, R.J. Severinsen, J.K. Buchanan, K.J. Shaffer, H.T. Jameson, N. Thennakoon, I. Leito, M. Lõkov, A. Kütt, R. Vianello, I. Despotović, N. Radić, P.G. Plieger, Synthesis and basicity studies of quinoline[7,8-*h*]quinoline derivatives, *J. Org. Chem.* 85 (2020) 11297–11308. <https://doi.org/10.1021/acs.joc.0c01428>
- [37] K.A. Kurnia, W. Setyaningsih, N. Darmawan, B. Yulianto, A comprehensive study on the impact of the substituent on pK_a of phenylboronic acid in aqueous and non-aqueous solutions: A computational approach, *J. Mol. Liq.* 326 (2021) 115321. <https://doi.org/10.1016/j.molliq.2021.115321>

- [38] M.D. Tissandier, K.A. Cowen, W.Y. Feng, E. Gundlach, M.H. Cohen, A.D. Earhart, J.V. Coe, T.R. Tuttle, The proton's absolute aqueous enthalpy and Gibbs free energy of solvation from cluster-ion solvation data, *J. Phys. Chem. A* 102 (1998) 7787–7794. <https://doi.org/10.1021/jp982638r>
- [39] M. Shkoor, H. Mehanna, A. Shabana, T. Farhat, A.D. Bani-Yaseen, Experimental and DFT/TD-DFT computational investigations of the solvent effect on the spectral properties of nitro substituted pyridino[3,4-*c*]coumarins. *J. Mol. Liq.* 313 (2020) 113509. <https://doi.org/10.1016/j.molliq.2020.113509>
- [40] Gaussian 16, Revision C.01, M.J. Frisch, G.W. Trucks, H.B. Schlegel, G.E. Scuseria, M.A. Robb, J.R. Cheeseman, G. Scalmani, V. Barone, G.A. Petersson, H. Nakatsuji, X. Li, M. Caricato, A.V. Marenich, J. Bloino, B.G. Janesko, R. Gomperts, B. Mennucci, H.P. Hratchian, J.V. Ortiz, A.F. Izmaylov, J.L. Sonnenberg, D. Williams-Young, F. Ding, F. Lipparini, F. Egidi, J. Goings, B. Peng, A. Petrone, T. Henderson, D. Ranasinghe, V.G. Zakrzewski, J. Gao, N. Rega, G. Zheng, W. Liang, M. Hada, M. Ehara, K. Toyota, R. Fukuda, J. Hasegawa, M. Ishida, T. Nakajima, Y. Honda, O. Kitao, H. Nakai, T. Vreven, K. Throssell, J.A. Montgomery Jr., J.E. Peralta, F. Ogliaro, M.J. Bearpark, J.J. Heyd, E.N. Brothers, K.N. Kudin, V.N. Staroverov, T.A. Keith, R. Kobayashi, J. Normand, K. Raghavachari, A.P. Rendell, J.C. Burant, S.S. Iyengar, J. Tomasi, M. Cossi, J.M. Millam, M. Klene, C. Adamo, R. Cammi, J.W. Ochterski, R.L. Martin, K. Morokuma, O. Farkas, J.B. Foresman, D.J. Fox, Gaussian, Inc., Wallingford CT, 2016.
- [41] I. Boček, K. Starčević, I. Novak Jovanović, R. Vianello, M. Hranjec, Novel imidazo[4,5-*b*]pyridine derived acrylonitriles: A combined experimental and computational study of their antioxidative potential, *J. Mol. Liq.* 342 (2021) 117527. <https://doi.org/10.1016/j.molliq.2021.117527>
- [42] E. Horak, R. Vianello, M. Hranjec, S. Krištafor, G.K. Zamola, I.M. Steinberg, Benzimidazole acrylonitriles as multifunctional push-pull chromophores: Spectral characterisation, protonation equilibria and nanoaggregation in aqueous solutions. *Spectrochim Acta A* 178 (2017) 225–233. <http://dx.doi.org/10.1016/j.saa.2017.02.011>
- [43] B. Valeur, *Molecular fluorescence-principles and applications*, Wiley-VCH, Weinheim, 2002.
- [44] A. Steinegger, O.S. Wolfbeis, S.M. Borisov, Optical Sensing and Imaging of pH Values: Spectroscopies, Materials, and Applications, *Chem Rev.* 120(22) (2020) 12357–12489. <https://doi.org/10.1021/acs.chemrev.0c00451>
- [45] M. Hranjec, E. Horak, D. Babić, S. Plavljanin, Z. Srdović, I.M. Steinberg, R. Vianello, N. Perin, Fluorescent benzimidazo[1,2-*a*]quinolines: synthesis, spectroscopic and computational studies of protonation equilibria and metal ion sensitivity, *New Journal of Chemistry* 41 (2017) 358–371. <https://doi.org/10.1039/c6nj02268e>

- [46] B. Wang, E.V. Anslyn, *Chemosensors: Principles, Strategies and Applications*, Wiley-VCH, Weinheim, 2011.
- [47] A.P. Demchenko, *Introduction to fluorescence sensing*, Springer, 2015. <https://doi.org/10.1007/978-3-319-20780-3>
- [48] L. Stroea, M. Murariu, V. Melinte, Fluorescence quenching study of new coumarin-derived fluorescent imidazole-based chemosensor, *J. Mol. Liq.* 318 (2020) 114316. <https://doi.org/10.1016/j.molliq.2020.114316>
- [49] M.J. Cook, A.R. Katritzky, P. Linda, R.D. Tack, Aromaticity and tautomerism. Part II. The 4-pyridone, 2-quinolone, and 1-isoquinolone series, *J. Chem. Soc., Perkin Trans. 2* (1973) 1080–1086.
- [50] M. Lõkov, S. Tshepelevitsh, A. Heering, P.G. Plieger, R. Vianello, I. Leito, On the basicity of conjugated nitrogen heterocycles in different media, *Eur. J. Org. Chem.* (2017) 4475–4489. <https://doi.org/10.1002/ejoc.201700749>
- [51] S. Tshepelevitsh, A. Kütt, M. Lõkov, I. Kaljurand, J. Saame, A. Heering, P. Plieger, R. Vianello, I. Leito, On the Basicity of Organic Bases in Different Media, *Eur. J. Org. Chem.* (2019) 6735–6748. <https://doi.org/10.1002/ejoc.201900956>
- [52] G. Yagil, The proton dissociation constant of pyrrole, indole and related compounds, *Tetrahedron* 23 (1967) 2855–2861. [https://doi.org/10.1016/0040-4020\(67\)85151-2](https://doi.org/10.1016/0040-4020(67)85151-2)
- [53] M.M. Fickling, A. Fischer, B.R. Mann, J. Packer, J. Vaughan, Hammett Substituent Constants for Electron-withdrawing Substituents: Dissociation of Phenols, Anilinium Ions and Dimethylanilinium Ions, *J. Am. Chem. Soc.* 81(16) (1959) 4226–4230. <https://doi.org/10.1021/ja01525a027>
- [54] C. Li, M.Z. Hoffman, One-Electron Redox Potentials of Phenols in Aqueous Solution, *J. Phys. Chem. B* 103 (1999) 6653–6656. <https://doi.org/10.1021/j100215a033>
- [55] O. S. Wolfbeis, Editorial: Probes, Sensors, and Labels: Why is Real Progress Slow? *Angew. Chem.* 52 (2013) 9864–9865. <https://doi.org/10.1002/anie.201305915>